Hindawi
European Journal of Cancer Care
Volume 2024, Article ID 1834636, 15 pages
https://doi.org/10.1155/2024/1834636

*Research Article*

# Identification of a Novel Circadian Rhythm-Related Signature for Predicting Prognosis and Therapies in Hepatocellular Carcinoma Based on Bulk and Single-Cell RNA Sequencing

**Gai Liu,[1,2] YuRong Luo,[1] JunHao Liu,[2] Ti Yang,[1,2] Zengxin Ma,[1,2] Jia Sun,[2,3] WenJun Zhou,[1,2] Hailiang Li,[2] Jianfan Wen ,[2] and Xiancheng Zeng [1,2]**

[1]*The Second School of Clinical Medicine, Southern Medical University, Guangzhou, China*
[2]*Department of Hepatobiliary-Pancreatic & Hernia Surgery, Guangdong Second Provincial General Hospital, Guangzhou, China*
[3]*Guangdong Second Provincial General Hospital, School of Medicine, Jinan University, Guangzhou, China*

Correspondence should be addressed to Jianfan Wen; wenjianfan927@163.com and Xiancheng Zeng; llyml2023@163.com

Received 21 September 2023; Revised 21 February 2024; Accepted 27 February 2024; Published 23 March 2024

Academic Editor: Pranshu Sahgal



*Background*. Circadian rhythm disruption involves tumorigenesis and tumor progression. However, the influences of circadian rhythm on the tumor microenvironment (TME) and the prognosis of hepatocellular carcinoma (HCC) are unknown. *Methods*. Bulk RNA-seq and single-cell RNA-seq from TCGA, ICGC, and GEO were used to comprehensively identify prognostic circadian control cells and circadian rhythm associated genes (CRRGs) using R and Python packages. Besides, the circadian rhythm-related prognostic signature was identified and validated. The biological function, immune infiltration, and therapeutic response associated with circadian rhythm-related (CR) risk were detected. *Results*. A total of 252 differentially expressed CRRGs in HCC were identified, and HCC with a high CR score revealed poor survival. We annotated 11 major cell types in TME; immune cells (B cells, myeloid, CD4+ cells, CD8+ cells, NK cells, Tregs) with high CR score, and hepatocyte, bio-potent cells, fibroblasts, and endothelial cells with low CR score were identified. Moreover, five CRRGs (RPL29, PFKFB3, RPS7, SLC6A6, and RPLP2) were selected and validated as the prognostic signature in HCC. The risk score was calculated based on the prognostic signature, and patients then were divided into high-risk and low-risk groups according to the median value of the risk score. High risk is linked to several metabolism-related pathways and canonical cancer-related pathways and is negatively associated with immunotherapeutic responses and positively associated with some chemotherapeutic drugs. *Conclusion*. Our finding provides the novel circadian rhythm-related prognostic signature and represents a novel viable "time-dependent" therapeutic option for HCC treatment.

## 1. Introduction

Hepatocellular carcinoma (HCC) stands as one of the most prevalent malignant liver cancers, accounting for 75%–85% of cases and ranking as the fourth leading cause of cancer-related deaths globally [1]. Hepatitis B virus (HBV) or hepatitis C virus (HCV) infection, aflatoxin-contaminated food, high alcohol consumption, smoking, obesity, non-alcoholic fatty live disease (NAFLD), and type 2 diabetes are the main risk factors that contribute to HCC development [2, 3]. Over the past decade, advancements in HCC management have significantly improved the overall survival and quality of life for patients [4]. Commonly, patients with early-stage HCC are often considered for surgical resection or transplantation. Those in the intermediate stage typically undergo the standard of care, involving transarterial chemoembolization. For patients in the advanced stage, systemic therapies with first-line and second-line drugs, such as atezolizumab (anti-PD-L1 antibody), bevacizumab (anti-VEGF antibody), sorafenib, and lenvatinib (tyrosine kinase inhibitors, TKIs), are accepted treatment options [5]. However, there are limited clinical benefits

because of the frequent development of resistance [6]. The tumor microenvironment (TME) of HCC is a complex and structured mixture characterized by abnormal angiogenesis, chronic inflammation, and dysregulated extracellular matrix (ECM) remodeling, which contribute to the hypoxia, immunosuppressive, and acidic microenvironment [7, 8]. The complex TME mediates the aggressive tumorigenesis, metastasis, therapeutic resistance, immune evasion, and recurrence of HCC [8–10]. Therefore, exploring the molecular mechanisms in the regulation of TME of HCC and then identifying novel therapeutic strategies that improve survival are the next major challenges in HCC.

The circadian clock is a complex cellular mechanism that sustains self-perpetuating oscillations with a 24-hour periodicity to control several cyclic physiological processes, and disrupting circadian rhythm results in numerous physiological disorders and diseases, including cancer [11, 12]. Emerging evidence has demonstrated that circadian clock-control metabolism is a hallmark of cancer, and circadian rhythm can be found as the novel therapeutic target [13–16]. Circadian rhythm plays a pivotal role in tumorigenesis and tumor progression by orchestrating various biological processes within cancer cells. These processes include cell proliferation, apoptosis, DNA repair, and metabolism. In addition, circadian rhythm influences the TME by shaping the cellular properties and interactions among various components, such as tumor-associated macrophages (TAMs), myeloid-derived suppressor cells (MDSCs), neutrophils, dendritic cells, T cells, natural killer (NK) cells, cancer-associated fibroblasts (CAFs), and endothelial cells [17, 18]. Given the tissue-specific properties of circadian clocks, the liver serves as a physiological hub for circadian regulation [19, 20]. The dysfunction of the hepatic circadian clock is implicated in the regulation of various liver functions, encompassing synthetic and metabolic processes related to glucose, lipids, bile acids, amino acids, and more [21]. The circadian clock genes contribute to tumor growth and aggressive [20, 22, 23]. Alterations of the circadian clock genes are associated with the prognosis of HCC patients [24]. The abovementioned evidence has demonstrated that circadian rhythm plays an important role in hepatocarcinogenesis.

In the present study, we integrated the single-cell RNA-seq (scRNA-seq) data and bulk RNA-seq data to comprehensively identify the prominent cell types and elucidate the cell-to-cell communication in TME that was influenced by circadian rhythm. Moreover, selecting the prognostic circadian rhythm-related genes (CRRGs) based on scRNA-seq data and bulk RNA-seq data analyses to construct a risk model for survival prediction and the biological functions, immune infiltration characteristics, and therapeutic responses associated with CR-risk score were investigated. Our finding elucidated the TME characteristics by circadian rhythm influences and provided novel potential therapeutic options for HCC treatment.

## 2. Materials and Methods

*2.1. Data Acquisition and Processing.* The mRNA expression data and corresponding clinical profiles of 369 HCCs in the TCGA-LIHC cohort, 232 HCCs in the LIRI-JP cohort, and 221 HCCs in the GSE14520 cohort were downloaded from The Cancer Genome Atlas (TCGA, https://www.cancer.gov/ccg/research/genome-sequencing/tcga), International Cancer Genome Consortium (ICGC, https://dcc.icgc.org/), and Gene Expression Omnibus (GEO, https://www.ncbi.nlm.nih.gov/geo/). As well as the single-cell RNA-seq (scRNA-seq) data of the GSE156625 cohort was obtained from the GEO database. A total of 85 circadian rhythm-related genes (CRRGs) were downloaded from the PathCards in GeneCards (https://pathcards.genecards.org/) (Table S1).

*2.2. Screening the Differentially Expressed Circadian Rhythm-Related Genes (CRRGs).* "Limma" package in R [25] was performed to screen the differentially expressed genes (DEGs) between HCCs and nontumors with the thresholds of $|\log_2 (\text{fold change, FC})| > 0.585$ and $P$ value of $<0.05$. The CRRGs further were identified by overlapping the DEGs and 85 CRRGs.

*2.3. Calculating the CR Score.* CR score for each sample in the TCGA-LIHC cohort was calculated using single-sample gene set enrichment analysis (ssGSEA) through the "GSVA" package in R [26]. The "survminer" package in R [27] was performed to select the optimal cutoff value according to the CR score of each sample, the survival time, and the survival status. The patients were divided into high- and low-CR score groups according to the optimal cutoff value. The overall survival analysis was performed between high- and low-CR score groups.

*2.4. Construction of a Weighted Gene Coexpression Network Analysis (WGCNA).* The "WGCNA" package in R was used to construct a coexpression network and identify the CR score-related modules and genes [28]. The samples in the TCGA-LIHC cohort were normalized, and the outlier samples were removed. The soft threshold power ($\beta$) was selected to ensure the network was scale-free, and the genes in the first quartile of variance were calculated by a power function. The adjacency matrix was then transformed into a topological overlap matrix (TOM), and the corresponding dissimilarity (1-TOM) also was calculated. The dynamic tree-cut method was used to identify the module by hierarchically clustering genes. A deepSplit value of 2 and a minimum size cutoff of 30 were selected as the distance measure for constructing the dendrogram. The significant modules were screened based on the correlation between CR score and modules by Pearson's correlation test. The gene expression profiles with module eigengenes (Mes) were

defined as a module membership (MM), and the correlation between outer features and gene expression profiles was defined as the gene significance (GS). The hub genes were identified that are located in the modules with the highest MM and highest GS values.

*2.5. Single-Cell RNA-Seq Data Analysis.* The normalized scRNA-seq data of the GSE156625 cohort was obtained from the GEO database, which comprised a total of 57, 25414 HCCs and 1 normal sample [29]. "Scanpy," a scalable Python-based package [30], was used for downstream analysis. Unified manifold approximation and projection (UMAP) was used for dimensionality reduction and cell clustering visualization [31]. The "AUCell" package in R [32] was performed to calculate CR scores for each cell type, and the cells were divided into high-CR score and low-CR score cell populations based on the median value of AUCell value. The differential gene expression between high-CR and low-CR score groups was identified using "scanpy.tl.rank_genes_groups" [30]. The "GSEApy" package was performed for biological function analysis [33].

*2.6. Construction and Validation of a Circadian Rhythm-Related Signature for Predicting Prognosis.* The intersected CRRGs between the DEGs from scRNA-seq data analysis and the hub genes from WGCNA were screened and visualized by a diagram analysis. A univariate Cox analysis was used to select the prognostic CRRGs in HCC. Then, the least absolute shrinkage and selection operator (LASSO) regression was performed using the "glmnet" package [34] to shrink the list of genes and to obtain the risk coefficients strongly linked to prognosis, and a risk model was further constructed. The risk score was calculated as follows: risk score = sum (each gene expression x the corresponding coefficient). HCC patients in TCGA-LIHC, LIRI-JP, and GSE14520 cohorts were divided into high-risk and low-risk groups with the median value of risk score. The overall survival curves were drawn using the Kaplan–Meier method by the "survminer" R package [35], and the performance of the risk model was evaluated by the area under the curve (AUC) values of the receiver operating characteristic (ROC) curves which were generated using "survivalROC" package in R [35]. In addition, GO and KEGG pathway enrichment analyses between high-risk and low-risk groups were performed using the "GSEApy" package in R [30].

*2.7. Patients and Specimens.* A total of 10 HCC patients and 7 healthy people at the Guangdong Second Provincial General Hospital were enrolled in this study between July 2023 and November 2023. All the patients had been diagnosed with primary HCC, and none had received any preoperative treatment. The patients underwent surgical resection, and serum samples were collected on the day of surgery. The protocol for collecting clinical samples was approved by the Ethics Committee of the Guangdong Second Provincial General Hospital (2023-KY-KZ-034-02), and the patients provided informed consent before samples were collected. The fresh specimens were obtained and immediately frozen in liquid nitrogen and then saved at −80°C for subsequent experiments.

*2.8. RNA Isolation and Real-Time PCR Assay.* Total RNA was extracted with TRIzol reagent (Takara, Dalian, China). Reverse transcription was performed with Prime-Script RT reagent Kit (DBI® Bioscience, Shanghai, China) according to the manufacturer's instructions. For real-time PCR analysis, the resultant cDNA products were amplified using SYBR Green qPCR Master Mix (DBI, Shanghai, China) in triplicates. Primer sequences of the genes analyzed were GAPDH: 5′-TGTTCGTCATGGGTGTGAAC-3′ and 5′-ATGGCATGGACTGTGGTCAT-3′; RPL29 : 5′-ACACCACACACAACCAGTCC-3′ and 5′-GCATTGTTGGCCTGCATCTT-3′; PFKFB3: 5′-GATGCCCTTCAGGAAAGCCT-3′ and 5′-GAACACTTTTGTGGGGACGC-3′; RPS7: 5′-CCAAGCGAAATTGTGGGCAA-3′ and 5′-CCTTGCCCGTGAGCTTCTTA-3′; SLC6A6: 5′-CCCAGGCTCTCTGAAATGGG-3′ and 5′-AGGAGCATGGCGAATGGAAA-3′; and RPLP2: 5′-CGACCGGCTCAACAAGGTTA-3′ and 5′-GGCTTTATTTGCAGGGGAGC-3′. GAPDH was used for normalization of the expression levels of each gene. The relative expression was quantified by using the $2^{-\Delta\Delta Ct}$ method.

*2.9. Construction of a Predictive Nomogram.* The risk score and clinical characteristics (such as age, sex, and clinical grade) were subjected to multivariate Cox regression to obtain the independent risk factor, and the relevant forest plot was drawn using the "ezcox" package in R [36]. A predictive nomogram was constructed using the "regplot" package in R [37] based on the independent risk factors. ROC curves were used to evaluate the performance of the predictive model. A calibration plot was drawn to calculate the efficiency of the predictive model using the "rms" package [38]. A decision curve was drawn to assess the ability of the predictive model by the "dcurves" package [39].

*2.10. Estimation of the Immune Cell Infiltration in the High-CR Risk and Low-CR Risk Groups.* A total of 28 immune cell-relevant gene sets were constructed according to the previous study [40]. ssGSEA was performed using the "GSVA" package in R [26] to calculate the immune infiltration score for each sample in the TCGA-LIHC cohort, and the differences between the high-risk and low-risk groups were tested using the Kruskal–Wallis test. Moreover, the differential expression of immune checkpoint-related genes between high-risk and low-risk groups was evaluated using the Kruskal–Wallis test.

*2.11. Evaluation of the Response to Immunotherapy and Chemotherapy in HCC.* Tumor immune dysfunction and exclusion (TIDE) was used to predict immune checkpoint blockade (ICB) response [41]. Immunophenoscore (IPS) also can be used to predict the response to immunotherapies including CTLA-4 and PD-1 blockers [40]. Here, the "tidepy" function in the Python package was performed to

evaluate the TIDE score of each sample in the TCGA-LIHC cohort [41], and the "IOBR" R package was performed to evaluate the immunophenoscore (IPS) of each sample in the TCGA-LIHC cohort [42]. The significant differences in TIDE score and IPS between high-risk and low-risk groups were detected using the Kruskal–Wallis test. Moreover, the half-maximal inhibitory concentration ($IC_{50}$) for patients with HCC based on the Genomics of Drug Sensitivity in Cancer (GDSC2) database (https://www.cancerrxgene.org) was calculated by the "oncoPredict" package in R, which was performed to predict drug response [43]. The differences in $\log_2$ ($IC_{50}$) between high-risk and low-risk groups were tested using the Kruskal–Wallis test.

*2.12. Statistical Analysis.* Statistical analyses were performed for all experiments with the GraphPad Prism software (Version 8.0, San Diego, CA). Results are presented as mean ± SD from at least 3 independent experiments. The statistical differences were calculated by using the Student's *t*-test. $^{*}P < 0.05$ versus the control group, $^{**}P < 0.01$ versus the control group, and $^{***}P < 0.001$ versus the control group.

## 3. Results

*3.1. High-CR Score Correlated with Poor Survival of HCC Patients.* The detailed flowchart of this study is shown in Figure S1. Among the TCGA-LIHC cohort, a total of 8831 DEGs (7793 upregulated and 1038 downregulated) were screened between HCCs and normal samples with the thresholds of $|\log_2 FC| > 0.585$ and $P$ value of <0.05 (Figures 1(a) and 1(b), and Table S2). Then, a total of 40 differentially expressed CRRGs were obtained (Figures 1(c) and 1(d) and Table S3). Circadian rhythm plays an important role in the regulation of complex physiological activities in HCC [44]. Therefore, the CR score for each sample in the TCGA-LIHC cohort was calculated using ssGSEA, and patients were distributed into high- and low-CR score groups based on the optimal cutoff value. The patients were divided into high- and low-CR score groups according to the optimal cutoff value, and the results suggested that patients in the high-CR score showed poorer survival time than those in the low-CR score group (Figure 1(e)). These findings suggested that dysregulation of circadian rhythm was associated with the differential prognosis in HCC.

*3.2. Identification of the Key Modules and Hub Genes Related to Circadian Rhythm.* WGCNA was constructed to identify the key modules and genes that were related to the circadian rhythm in HCC [45]. After normalization and removing the outlier samples (Figure 2(a)), the coexpression network was constructed with the $\beta$-value as 14, and the scale-free $R^2$ was equal to 0.8, and a total of eleven different coexpression modules with different colors finally were identified (Figures 2(b) and 2(c)). The module-CR score analysis indicated that brown and green modules revealed the highest correlations with the CR score (Figure 2(d)). A total of 252 hub genes related to circadian rhythm were identified according to the threshold of MM >0.6 and GS >0.3 (Figures 2(e)–2(g) and Table S4).

Identification of the CR-score-related cell subpopulations.

The normalized scRNA-seq data (GSE156625) were performed using UMAP dimensionality reduction to identify 28 Louvain clusters using the "Scanpy" package (Figure 3(a)). Then, 28 Louvain clusters were annotated into 11 major cell types based on the data source article, including hepatocytes, fibroblasts, bipotent cells, endothelial cells, B cells, myeloid, CD4+ cells, CD8+ cells, natural killer (NK) cells, Tregs, and mast cells (Figure 3(a)). The GO annotation enrichment analysis based on the DEGs of each population indicated that distinct cell clusters were involved in different biological processes (Figure 3(b)). For example, B cells were associated with the regulation of humoral immune response, complement activation, and immune effector process. CD4+ T cells, CD8+ T cells, and NK cells were involved in post-translational protein modification. CD4+ T cells and Tregs were involved in receptor-mediated endocytosis. CD8+ T cells, NK cells, and Tregs were involved in platelet degranulation. NK cells and Tregs were involved in regulated exocytosis. Then, to explore the CRRG expression characteristics in HCC, the CR score of each cell was calculated using the AUCell R package (Figure 3(c)). All cells were distributed into the high-CR score and low-CR score groups based on the median value of AUCell value; hepatocyte, bipotent cells, fibroblasts, and endothelial cells were distributed into the low-CR score group; and most immune cells were distributed into the high-CR score group (Figure 3(c)). A total of 2792 DEGs (2649 upregulated and 143 downregulated) were identified between the high-CR score and low-CR score groups (Table S5). GO and KEGG pathway enrichment analyses based on the DEGs between the high-CR score and low-CR score groups are exhibited in Figures 3(d) and 3(e), and upregulated DEGs are involved in cytoplasmic translation and cotranslational protein targeting the membrane. The downregulated DEGs were associated with prostanoid and prostaglandin metabolic processes. These findings suggested that immune cells in the TME were more likely to be influenced by the circadian rhythm.

*3.3. Construction and Validation of a Circadian Rhythm-Related Signature.* To explore the prognostic values of CRRGs in HCCs, a total of 44 CRRGs were obtained by overlapping CRRGs from WGCNA and scRNA-seq analyses (Figure 4(a) and Table S6). Univariate Cox analysis indicated that 21 CRRGs were associated with prognosis (Figure 4(b)). Then, five CRRGs (RPL29, PFKFB3, RPS7, SLC6A6, and RPLP2) were selected as the prognostic signature using the LASSO regression analysis (Figures 4(c)–4(e)). Then, the CR-related risk scores were calculated based on the prognostic gene expression and corresponding coefficients, and HCC patients were classed into high-risk and low-risk groups according to the median value of risk scores both in training cohort (TCGA-LIHC, Figures 4(f)–4(h)) and external validation cohorts (LIRI-JP cohort and GSE14520,

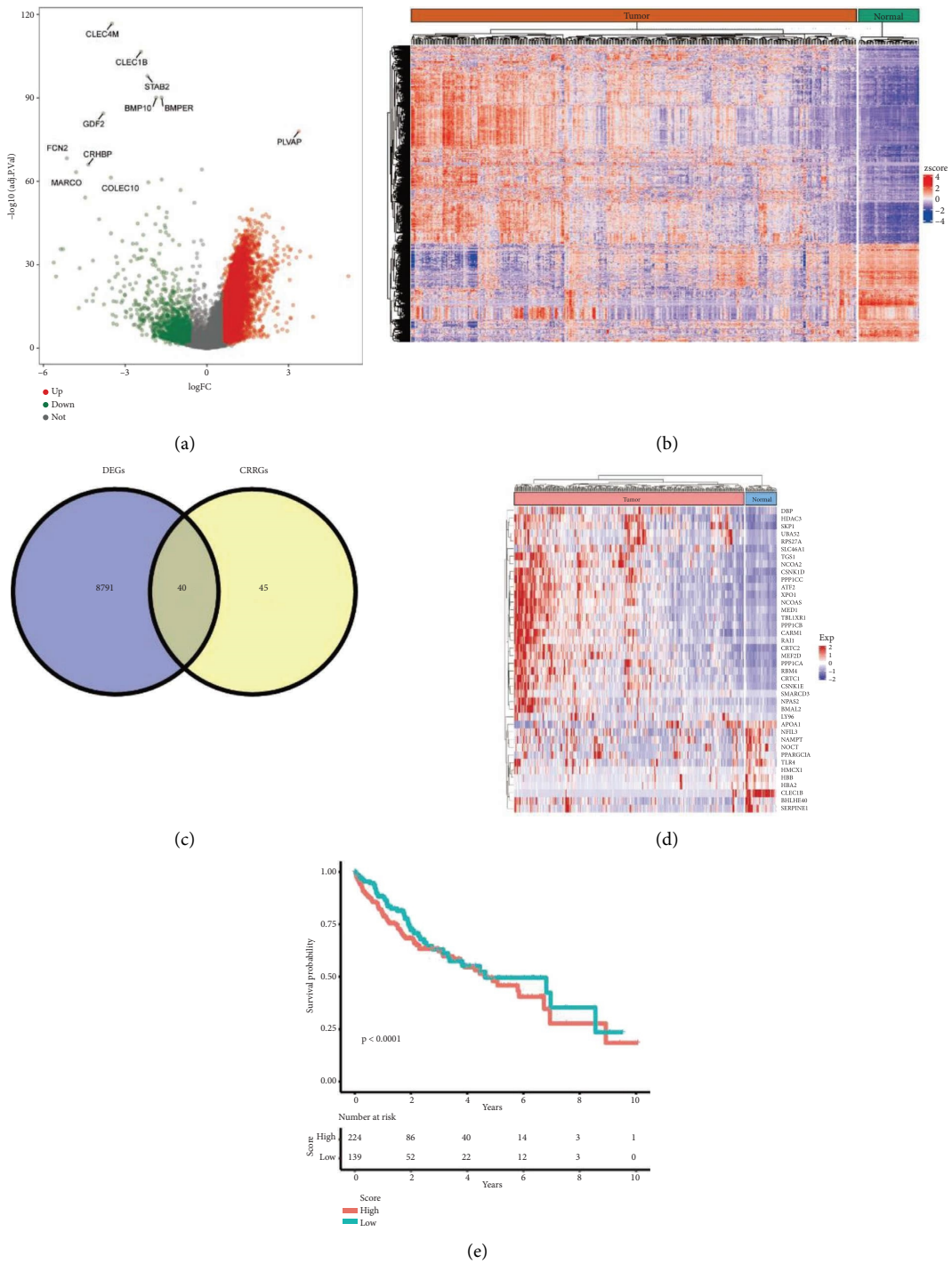


Figure 1: High-CR score correlated with poor survival of HCC patients. (a) The volcano plot of DEGs between tumor and normal samples of HCCs in the TCGA-LIHC cohort. (b) Heatmap of DEGs between tumor and normal samples of HCCs in the TCGA-LIHC cohort. (c) Venn plot of the differentially expressed CRRGs by overlapping DEGs and CRRGs. (d) Heatmap of 40 intersected CRRGs between tumor and normal samples of HCCs in the TCGA-LIHC cohort. (e) Kaplan–Meier plots for HCCs in high-CR score and low-CR score groups.

Figures 4(k)–4(m) and 4(p)–4(r)). The Kaplan–Meier survival curves indicated that the high-risk group showed worse survival than the low-risk group (Figures 4(i), 4(n), and 4(s)). AUC values of the ROC curves for the 1-, 3-, and 5-year survival analyses indicated the accuracy of the model for the survival prediction (Figures 4(j), 4(o), and 4(t)).

*3.4. qPCR Validation of the Expression of Circadian Rhythm-Related Signature.* To validate the expression of the circadian rhythm-related signature (RPL29, PFKFB3, RPS7, SLC6A6, and RPLP2) in HCC, qPCR was conducted to examine the mRNA expression of RPL29, PFKFB3, RPS7, SLC6A6, and RPLP2. As shown in Figures 5(a)–5(e), we

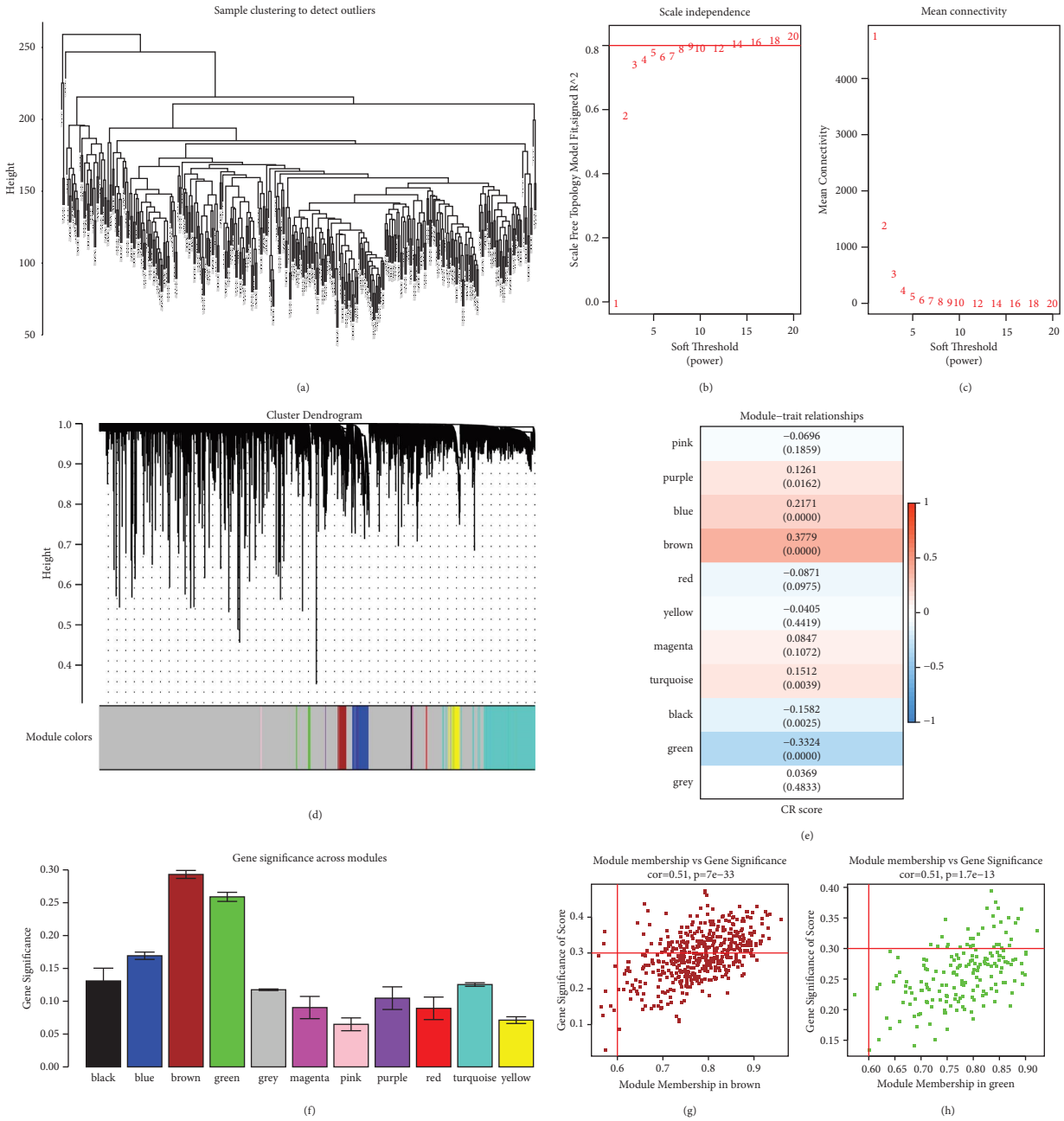


FIGURE 2: Identification of the key modules and hub genes related to circadian rhythm. (a) Sample clustering to identify the outliers. (b) The scale-free index for soft-thresholding powers. (c) A dendrogram based on hierarchical clustering with optimal soft thresholds. (d) Heatmap of the correlation between modules and features (CR score). (e) The histogram of the gene significance (GS) across modules. (f, g) Scatter plot of the correlation between module membership (MM) and gene significance (GS) of score in brown and green modules, respectively.

found that the PFKFB3, RPS7, RPL29, RPLP2, and SLC6A6 were upregulated in HCC samples compared with controls. These results indicated that RPL29, PFKFB3, RPS7, SLC6A6, and RPLP2 might act as risk factors in HCC.

*3.5. Development of a Predictive Nomogram.* We incorporated the clinical characteristics into the univariate and multivariate Cox models to identify the independent risk factors in HCC, and the results suggested that risk score was selected as the independent risk factor of HCC (Figures 6(a) and 6(b)). Therefore, a nomogram was constructed by combining risk score and clinical characteristics (Figure 6(c)). The calibration curves indicated the efficiency of the nomogram for survival prediction (Figure 6(d)). Time-dependent ROC curves indicated the accuracy of the nomogram for survival prediction (Figure 6(e)). The DCA curves revealed the discriminative ability of the nomogram for survival prediction (Figure 6(f)).

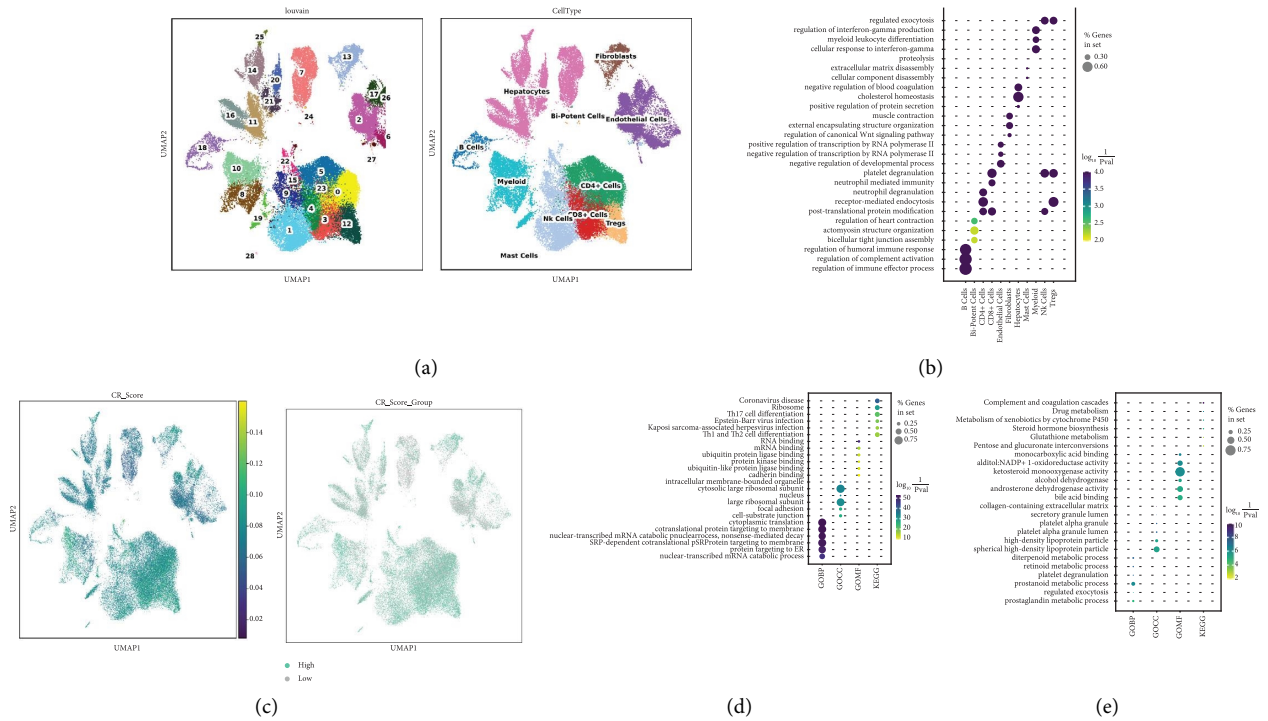


Figure 3: Dimensionality reduction, cell annotation, and identification of the CR score-related cell subpopulations. (a) Left: the UMAP of the 28 cell clusters. Right: the UMAP of 11 cell types was annotated by different markers. (b) The bubble plot shows the GO-BP analysis of DEGs for each cell type. (c) Left: the UMAP of the CR score for each cell type. Right: the UMAP of the cell types distributed into the high-CR score and low-CR score groups. (d, e) The bubble plot shows the GO (BP, CC, and MF) and KEGG enrichment analyses based on upregulated and downregulated DEGs between high-CR score and low-CR score groups, respectively.

*3.6. Biological Function Analyses.* We also investigated the biological function between high-risk and low-risk groups using GSEA. The GO analysis indicated that CR risk was involved in the cellular protein metabolic process, focal adhesion, steroid hydroxylase activity, and cell-substrate junction (Figures 7(a)–7(c)). The KEGG pathway enrichment analysis indicated that CR risk was linked to several metabolism-related pathways, such as fatty acid, tryptophan, tyrosine, glycine, serine, threonine, retinol, and bile acid metabolisms, and other enrichment pathways including RNA transport, DNA repair, and Wnt-beta catenin signaling pathway (Figure 7(d)). Furthermore, the hallmark pathway enrichment analysis revealed that CR risk was connected to several tumorigenesis pathways, such as the Wnt-beta catenin signaling pathway, p53 pathway, IL-2/STAT5 signaling pathway, mTORC1 signaling pathway, and PI3K/AKT/mTOR signaling pathway (Figure 7(e)).

## 4. Description of CR-Risk Score Relevant Tumor Immune Infiltration Landscape

We also described the immune cell landscape between high-risk and low-risk groups using ssGSEA. As shown in Figures 8(a) and 8(b), we found that most adaptive immune cells, such as the activated dendritic cells, CD56dim NK cells, immature dendritic cells, MDSC, macrophage, mast cell, NK T cells, and plasmacytoid dendritic cells, were significantly enriched in the high-risk group than in the low-risk group. Moreover, the innate immune cells also revealed a similar outcome, and the activated B cells, activated CD4+ T cells, central memory CD4+ T cells, central memory CD8+ T cells, effector memory CD4+ T cells, immature B cells, memory B cells, regulatory T cells, T follicular helper cells, Type17 T helper cells, and Type2 T helper cells also increased in the high-risk group than in the low-risk group (Figures 8(c) and 8(d)). These results were consistent with the scRNA-seq data analysis, in which CR played an important role in the regulation of the tumor environment.

*4.1. Prediction of the Response to Immunotherapy and Chemotherapy in High-Risk and Low-Risk Groups.* Next, we explored the immune checkpoint-related genes (ICRGs) expression between high-risk and low-risk groups, results showed that the upregulated ICRGs (BTLA, BTN2A1, CD160, CD209, CD226, CD27, CD276, CD28, CD40LG, CD47, CD70, CD80, CD86, CD96, CTLA4, HAVCR2, HLA-DRB1, ICOS, IDO1, LAG3, LGALS9, PDCD1, PDCD1LG2, TIGIT, TNFRSF14, TNFRSF18, TNFRSF4, TNFRSF9, TNFSF18, TNFSF4, and TNFSF9) were found in high-risk group compared with low-risk groups (Figures 9(a) and 9(b)). Then, we investigated the TIDE value and IPS, and the results indicated that higher TIDE value and lower IPS were observed in the high-risk group than in the low-risk group (Figures 9(c) and 9(d)). These results implied that high-risk scores were associated with a negative response to immunotherapy. We also investigated the distinction of

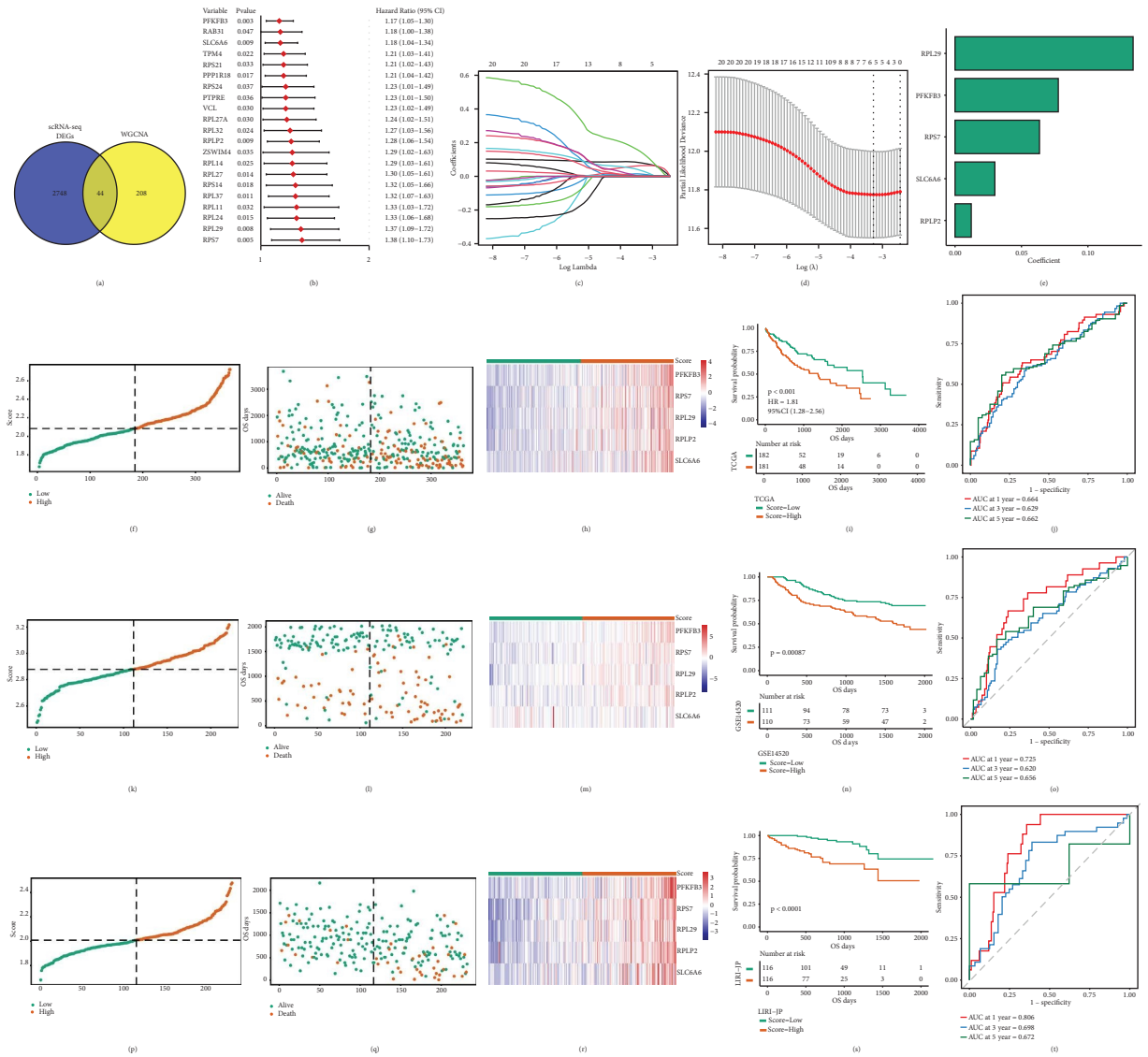

FIGURE 4: Construction and validation of a circadian rhythm-related signature. (a) Venn plot of the differentially expressed CRRGs by overlapping DEGs from scRNA-seq and bulk RNA-seq data. (b) The forest plot shows the prognostic CRRGs by univariate Cox analysis. (c) The trajectory of each independent variable with lambda. (d) Plots of the coefficient distributions for the logarithmic (lambda) series for parameter selection (lambda). (e) The selected prognostic genes and corresponding coefficients. (f, k, and p) The survival status of patients and risk score of the TCGA-LIHC cohort, LIRI-JP cohort, and GSE14520 cohort. (g, l, and q) The survival status of the patients with high-risk and low-risk score groups in the TCGA-LIHC cohort, LIRI-JP cohort, and GSE14520 cohort. (h, m, and r) The heatmap of the five CRRGs between high-risk and low-risk score groups in the TCGA-LIHC cohort, LIRI-JP cohort, and GSE14520 cohort. (i, n, and s) Kaplan–Meier plot for HCCs in the high-CR score and low-CR score groups of the TCGA-LIHC cohort, LIRI-JP cohort, and GSE14520 cohort. (j, o, and t) ROC curves for 1-, 3-, and 5-year survival prediction in the TCGA-LIHC cohort, LIRI-JP cohort, and GSE14520 cohort.

chemotherapy sensitivity between the high-risk group and the low-risk group, as shown in Figures 9(e) and 9(f), lower $IC_{50}$ values of MK-1775 (adavosertib), paclitaxel, pevonedistat, ULK1_4989, vinblastine, and vinorelbine in the high-risk group than the low-risk group. The results indicated that more chemotherapy sensitivity was found in high-risk scores compared with the low-risk score group.

## 5. Discussion

The circadian clock, an endogenous timekeeper system, consists of both master and peripheral clock genes, orchestrating various biological processes. Disruption of the circadian rhythm detrimentally impacts physiology and poses global health threats, contributing to proliferative, metabolic, and immune diseases [46, 47]. Circadian rhythm-regulated metabolism is a novel hallmark cancer and involves hepatocarcinogenesis, progression, metastasis, treatment outcomes, recurrences, and survival [48–51]. Increasing research suggests that circadian rhythm disruption is associated with the risk and prognosis of colorectal cancer [52]. Moreover, circadian rhythm disruption accelerates cancer growth, worse survival, and chemoresistance in pancreatic cancer [53]. Most studies conducted

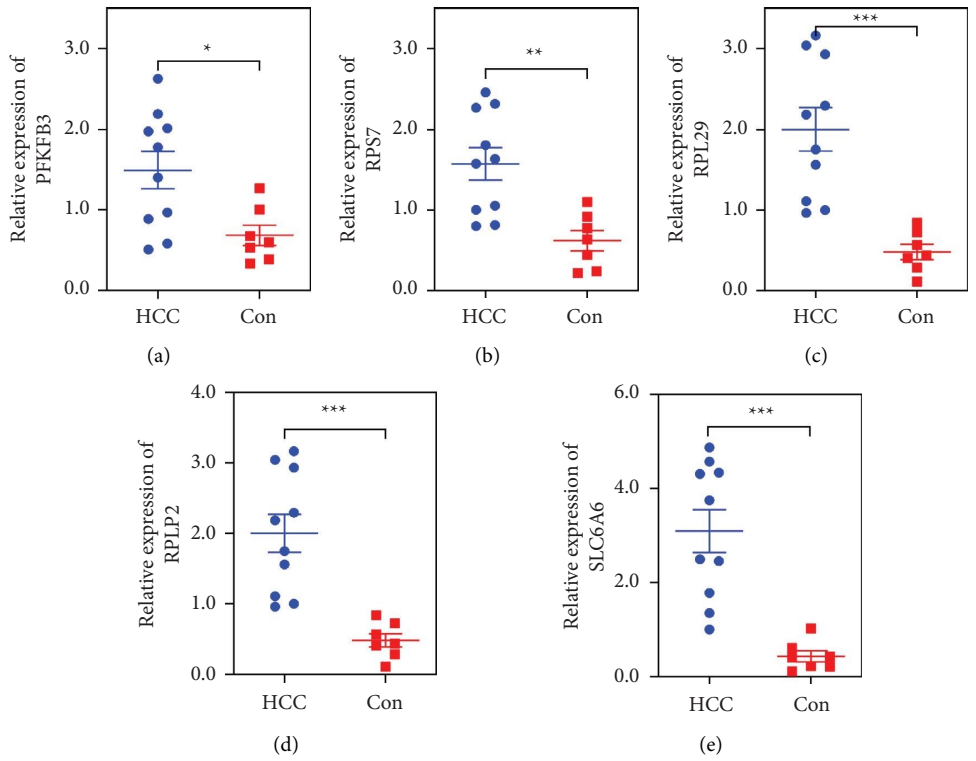


Figure 5: qPCR validation of the expression of circadian rhythm-related signature. (a–e) Scatter plots show the differential expression of PFKFB3, RPS7, RPL29, RPLP2, and SLC6A6. $^{*}P < 0.05$ versus the control group, $^{**}P < 0.01$ versus the control group, and $^{***}P < 0.001$ versus the control group.

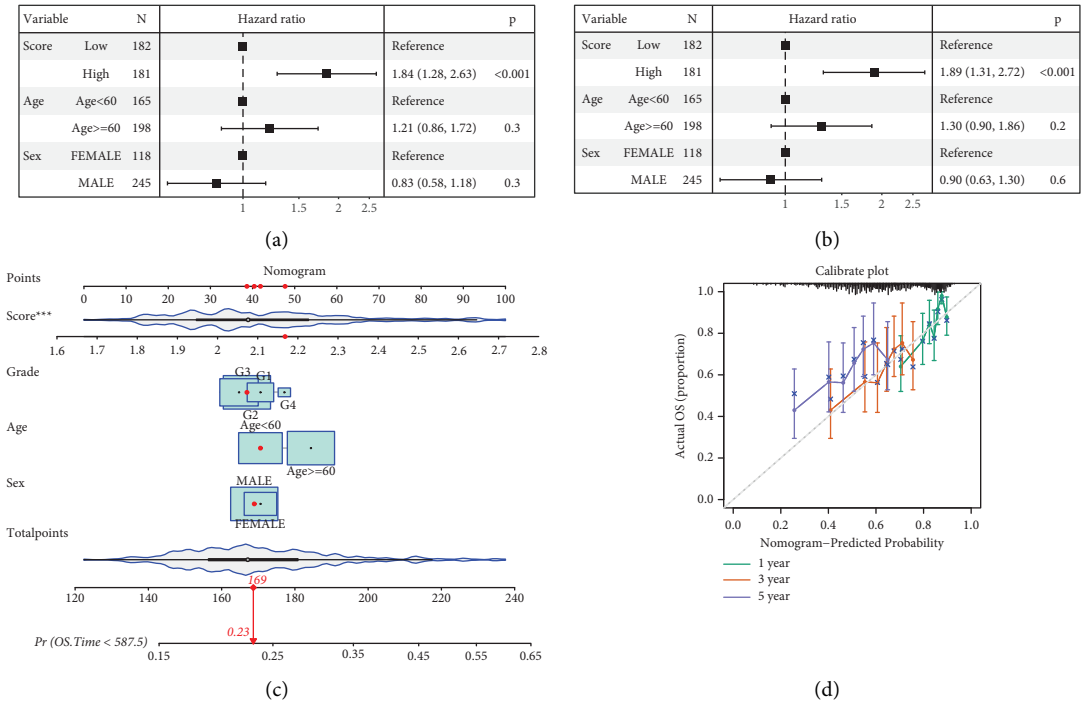


Figure 6: Continued.

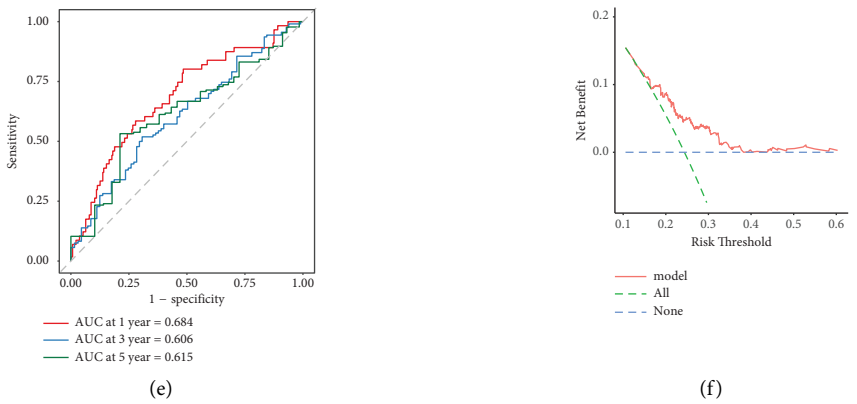


(e) (f)

Figure 6: Development of a predictive nomogram. (a, b) Univariate and multivariate Cox analyses were performed to identify independent risk factors. (c) A nomogram for survival prediction based on risk factors and clinical characteristics. (d–f) The calibration curve, DCA curve, and the time-dependent ROC curve were used to evaluate the efficiency, predictive ability, and performance of the predictive model.

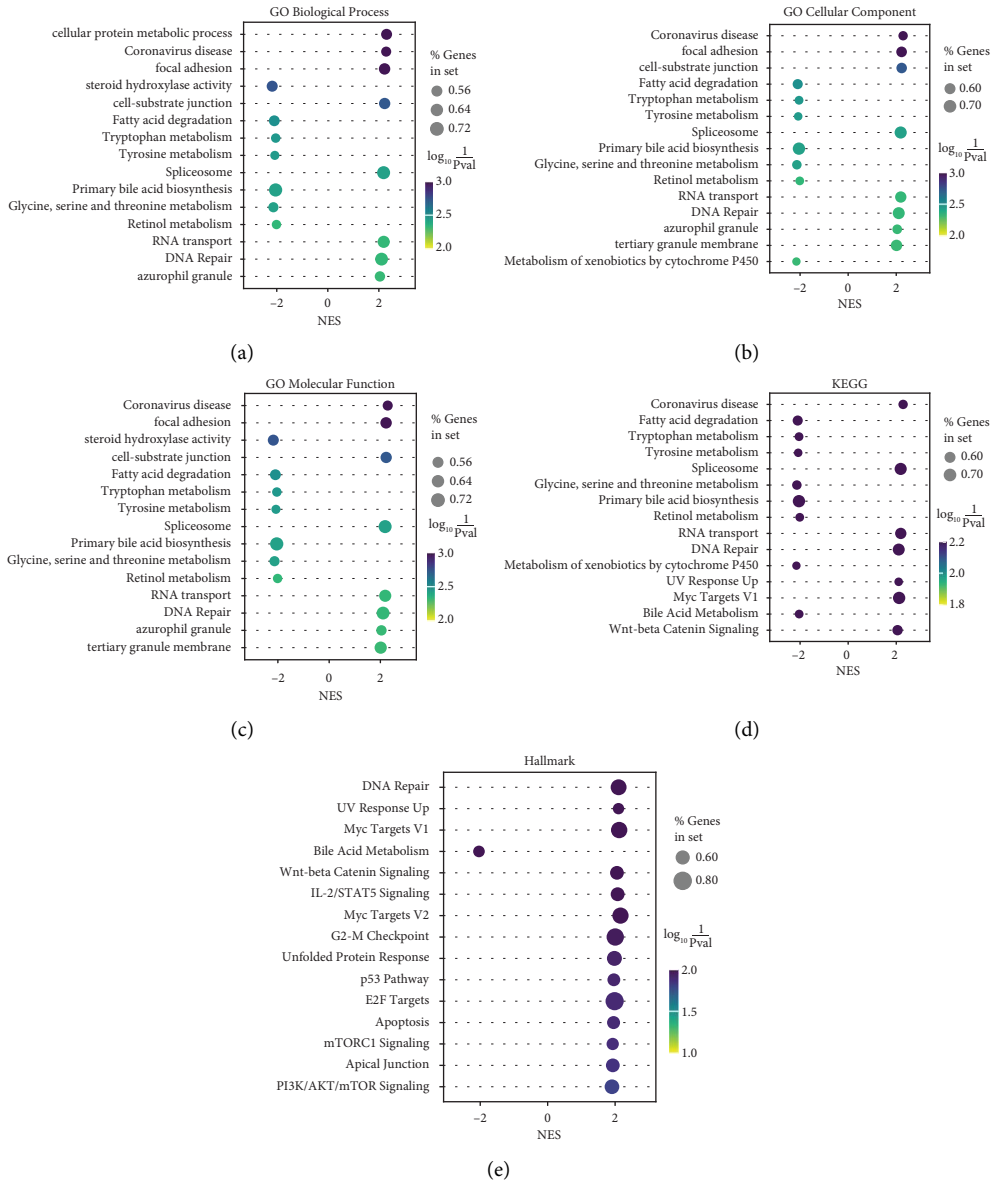


Figure 7: Biological function analyses. (a–c) Bubble plots of the GO enrichment analysis, including BP, CC, and MF. (d) Bubble plots of the KEGG pathway enrichment analysis. (e) Bubble plots of the hallmark pathway enrichment analysis.

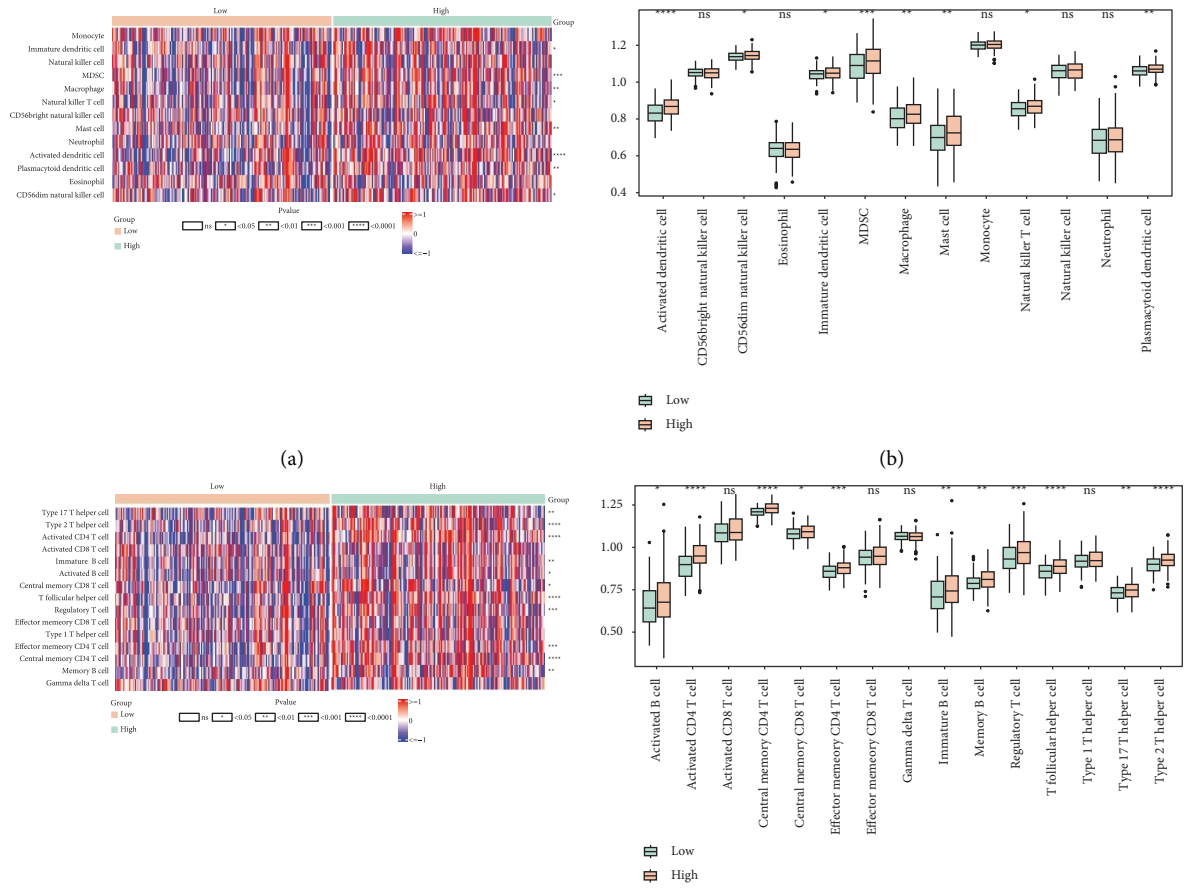


FIGURE 8: Description of CR-risk score relevant tumor immune infiltration landscape. (a, b) The differentially infiltrated native immune cells between high-risk and low-risk groups. (c, d) The differentially infiltrated adaptive immune cells between high-risk and low-risk groups.

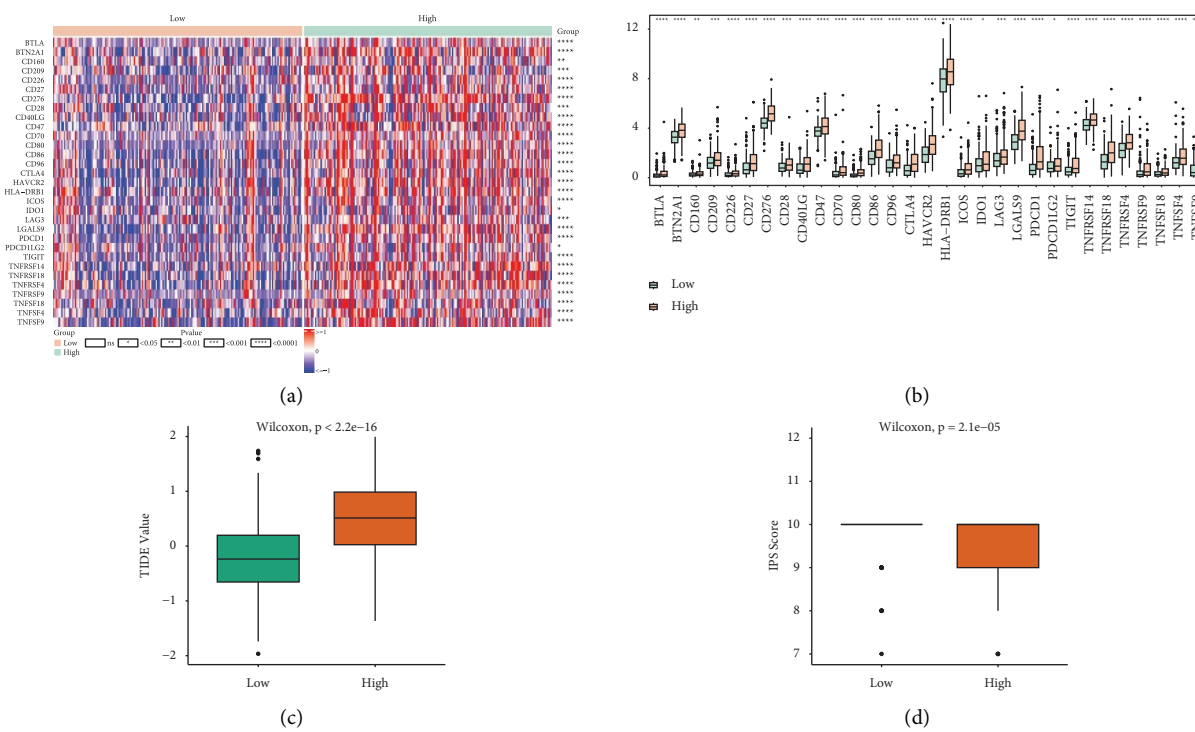


FIGURE 9: Continued.

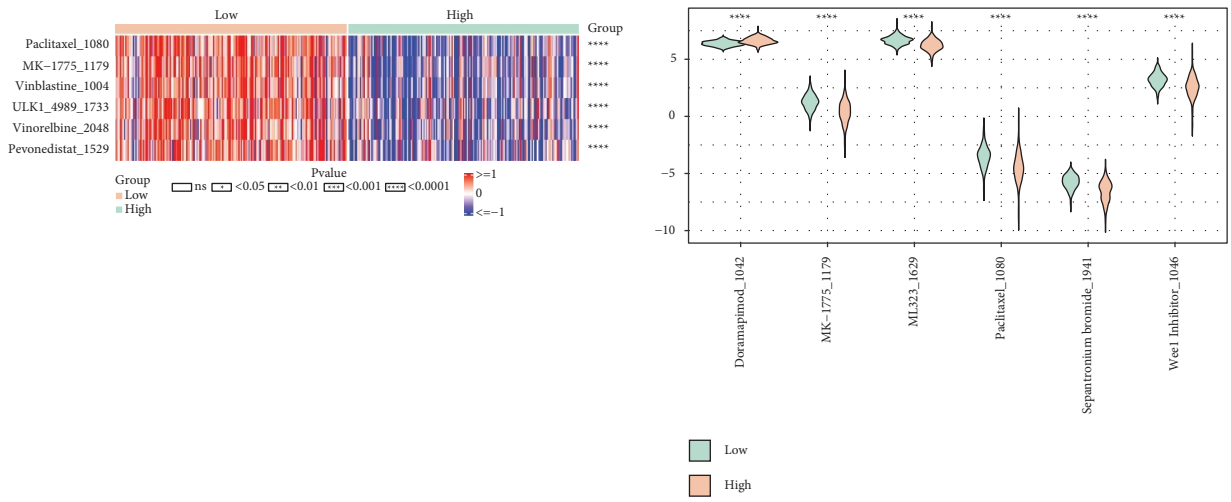


(e) (f)

Figure 9: Prediction of the response to immunotherapy and chemotherapy in high-risk and low-risk groups. (a, b) Heatmap and histogram of the differentially expressed immune checkpoint-related genes between high-risk and low-risk groups. (c, d) Histogram of the differentially expressed TIDE value and IPS between high-risk and low-risk groups. (e, f) The differential $IC_{50}$ values of chemotherapeutic drugs between high-risk and low-risk groups.

on the influences of circadian rhythm so far have focused on hub circadian clock genes that observed expression changes in the experimental detection results. However, a large number of the CRRGs that contribute to tumorigenesis and development are still unknown. Thus, in the present study, we comprehensively and intensively investigated the hub CRRGs and their regulatory mechanisms in HCC.

First, we identified the differentially expressed CRRGs in HCC and demonstrated that the differential expression of CRRGs is involved in survival. Therefore, we further screened the 252 hub genes that are associated with circadian rhythm. Meanwhile, we also investigated the landscape of the TME based on scRNA-seq data. We found that 11 major cell types, including hepatocytes, fibroblasts, bipotent cells, endothelial cells, B cells, myeloid, CD4+ cells, CD8+ cells, NK cells, and Tregs, were identified, and those genes were enriched in different biological processes. With the CR score calculation, all cells were clustered into high-CR score and low-CR score groups according to the median value of the CR score, and hepatocyte, bi-potent cells, fibroblasts, and endothelial cells were distributed into the low-CR score group, and most of the immune cells (B cells, myeloid, CD4+ cells, CD8+ cells, NK cells, and Tregs) were distributed into the high-CR score group. These data indicated that immune cells were strongly influenced by the circadian rhythm. Cancer-immunity cycle is a circulation system in TME that is composed of several major steps such as cancer cell antigen release and presentation, priming and activation of effector immunity cells, tracking and infiltration of immunity to tumors, and elimination of cancer cells [54]. It has been found that both the innate and adaptive arms of immunity in the TME possess circadian rhythmicity and have been linked to antitumor response [55–62]. Our results supported the abovementioned research findings that immune cells in the TME are regulated by circadian rhythmicity.

The abovementioned finding reminded us that circadian rhythm is involved in tumor growth, the outcome of treatment, and survival. Thus, we further investigated the prognostic values of CRRGs in HCC. By integrating scRNA-seq data and bulk RNA-seq data analyses, five CRRGs (RPL29, PFKFB3, RPS7, SLC6A6, and RPLP2) were selected and validated as the prognostic signature in HCC. Moreover, the experimental results also demonstrated the significant differential expression of five prognostic CRRGs. HCC patients were divided into high-risk and low-risk groups based on the median value of risk score. We also found a high-CR risk score linked to several metabolism-related pathways and canonical cancer-related pathways, such as the Wnt-beta catenin signaling pathway, p53 pathway, and PI3K/AKT/mTOR signaling pathway. Besides, a high-CR risk score not only promoted the increased proportions of innate and adaptive immune cells but also negatively associated with immunotherapeutic responses and positively associated with some chemotherapeutic drugs, including MK-1775 (adavosertib), paclitaxel, pevonedistat, ULK1_4989, vinblastine, and vinorelbine. Previous studies have demonstrated that circadian clock-control metabolism is a hallmark of cancer [12], and understanding the regulatory mechanisms of circadian rhythm links to the tumor immune microenvironment and metabolism could provide therapeutic benefits against tumors [63].

## 6. Conclusion

In conclusion, we integrated scRNA-seq data and bulk RNA-seq data to comprehensively explore the immune characteristics in TME and identify the prognostic CRRGs used for survival prediction. Our data provided novel "time-dependent" therapeutic options for HCC treatment.

## Data Availability

Publicly available datasets were analyzed in the present study. This data can be found here: The Cancer Genome Atlas (TCGA, https://www.cancer.gov/ccg/research/genome-sequencing/tcga), the International Cancer Genome Consortium (ICGC, https://dcc.icgc.org/), the Gene Expression Omnibus (GEO, https://www.ncbi.nlm.nih.gov/geo/), and the GeneCards (https://pathcards.genecards.org/).

## Ethical Approval

This study was approved by the Ethics Committee of the Guangdong Second Provincial General Hospital (2023-KY-KZ-034-02).

## Conflicts of Interest

The authors declare that they have no conflicts of interest.

## Authors' Contributions

GL wrote the manuscript, collected the data, and conceptualised and designed the study. YR and JHL conceptualised, designed, analyzed, and interpreted the study. TY wrote the manuscript, performed the critical revision of the manuscript, and developed the methodology. ZXM performed the formal analysis and critically revised the manuscript. JS, WJZ, and HLL critically revised the manuscript. JFW and XCZ conceptualised and designed the study and performed the critical revision. All authors contributed to the study and approved the submitted version. Gai Liu, YuRong Luo, and JunHao Liu are the co-first authors.

## Acknowledgments

This work was supported by the Guangdong Natural Science Foundation (Grant no. 2018A0303130184), the Science and Technology Projects in Guangzhou (Grant no. 202201020270), the Hospital Fund of Guangdong Second Provincial General Hospital (Grant no. 3D-A2020005), the Technology Projects in Guangzhou (Grant nos. 2023A03J0274 and 202102021064), and the Doctoral Workstation Foundation of Guangdong Second Provincial General Hospital (Grant no. 2021BSG8011).

## Supplementary Materials

Supplementary Figure 1: the workflow of the study design. Table S1: circadian rhythm-related genes (CRRGs) from the GeneCards. Table S2: DEGs between HCCs and normal samples in the TCGA-LIHC cohort ($|\log_2 FC| > 0.585$ and $P < 0.05$). Table S3: Venn analysis of the 40 intersected CRRGAs between CRRGs from GeneCards and DEGs from the TCGA-LIHC cohort. Table S4: identification of the hub genes based on WGCNA. Table S5: DEGs between high-CR score and low-CR score groups in the GSE156625 dataset ($|\log_2 FC| > 0.585$ and $P < 0.05$). Table S6: Venn analysis of the 44 intersected CRRCs between CRRGs from WGCNA and scRNA-seq data analysis. (*Supplementary Materials*)

## References

[1] H. Sung, J. Ferlay, R. L. Siegel et al., "Global cancer statistics 2020: GLOBOCAN estimates of incidence and mortality worldwide for 36 cancers in 185 countries," *CA: A Cancer Journal for Clinicians*, vol. 71, no. 3, pp. 209–249, 2021.

[2] L. Gravitz, "Liver cancer," *Nature*, vol. 516, no. 7529, 2014.

[3] A. Marengo, C. Rosso, and E. Bugianesi, "Liver cancer: connections with obesity, fatty liver, and cirrhosis," *Annual Review of Medicine*, vol. 67, no. 1, pp. 103–117, 2016.

[4] A. Forner, M. Reig, and J. Bruix, "Hepatocellular carcinoma," *The Lancet*, vol. 391, no. 10127, pp. 1301–1314, 2018.

[5] J. Balogh, "Hepatocellular carcinoma," *Nature Reviews Disease Primers*, vol. 7, no. 1, p. 7, 2021.

[6] L. Li, H. T. Liu, Y. X. Teng et al., "Second-line treatment options for hepatocellular carcinoma: current state and challenges for the future," *Expert Opinion on Investigational Drugs*, vol. 31, no. 11, pp. 1151–1167, 2022.

[7] K. Oura, A. Morishita, J. Tani, and T. Masaki, "Tumor immune microenvironment and immunosuppressive therapy in hepatocellular carcinoma: a review," *International Journal of Molecular Sciences*, vol. 22, no. 11, p. 5801, 2021.

[8] R. Donne and A. Lujambio, "The liver cancer immune microenvironment: therapeutic implications for hepatocellular carcinoma," *Hepatology*, vol. 77, no. 5, pp. 1773–1796, 2023.

[9] Z. Sas, E. Cendrowicz, I. Weinhäuser, and T. P. Rygiel, "Tumor microenvironment of hepatocellular carcinoma: challenges and opportunities for new treatment options," *International Journal of Molecular Sciences*, vol. 23, no. 7, p. 3778, 2022.

[10] C. Chen, Z. Wang, Y. Ding, and Y. Qin, "Tumor microenvironment-mediated immune evasion in hepatocellular carcinoma," *Frontiers in Immunology*, vol. 14, Article ID 1133308, 2023.

[11] A. R. Neves, T. Albuquerque, T. Quintela, and D. Costa, "Circadian rhythm and disease: relationship, new insights, and future perspectives," *Journal of Cellular Physiology*, vol. 237, no. 8, pp. 3239–3256, 2022.

[12] S. Masri and P. Sassone-Corsi, "The emerging link between cancer, metabolism, and circadian rhythms," *Nature Medicine*, vol. 24, no. 12, pp. 1795–1803, 2018.

[13] K. Kinouchi and P. Sassone-Corsi, "Metabolic rivalry: circadian homeostasis and tumorigenesis," *Nature Reviews Cancer*, vol. 20, no. 11, pp. 645–661, 2020.

[14] W. Ruan, X. Yuan, and H. K. Eltzschig, "Circadian rhythm as a therapeutic target," *Nature Reviews Drug Discovery*, vol. 20, no. 4, pp. 287–307, 2021.

[15] G. Sulli, M. T. Y. Lam, and S. Panda, "Interplay between circadian clock and cancer: new frontiers for cancer treatment," *Trends in Cancer*, vol. 5, no. 8, pp. 475–494, 2019.

[16] A. Verlande and S. Masri, "Circadian clocks and cancer: timekeeping governs cellular metabolism," *Trends in Endocrinology and Metabolism*, vol. 30, no. 7, pp. 445–458, 2019.

[17] W. Xuan, F. Khan, C. D. James, A. B. Heimberger, M. S. Lesniak, and P. Chen, "Circadian regulation of cancer cell and tumor microenvironment crosstalk," *Trends in Cell Biology*, vol. 31, no. 11, pp. 940–950, 2021.

[18] D. F. Quail and J. A. Joyce, "Microenvironmental regulation of tumor progression and metastasis," *Nature Medicine*, vol. 19, no. 11, pp. 1423–1437, 2013.

[19] M. Qu, H. Qu, Z. Jia, and S. A. Kay, "HNF4A defines tissue-specific circadian rhythms by beaconing BMAL1::CLOCK chromatin binding and shaping the rhythmic chromatin landscape," *Nature Communications*, vol. 12, no. 1, p. 6350, 2021.

[20] M. Qu, G. Zhang, H. Qu et al., "Circadian regulator BMAL1::CLOCK promotes cell proliferation in hepatocellular carcinoma by controlling apoptosis and cell cycle," *Proceedings of the National Academy of Sciences of the U S A*, vol. 120, no. 2, 2023.

[21] A. Mukherji, S. M. Bailey, B. Staels, and T. F. Baumert, "The circadian clock and liver function in health and disease," *Journal of Hepatology*, vol. 71, no. 1, pp. 200–211, 2019.

[22] S. Chen, L. Wang, B. Yao, Q. Liu, and C. Guo, "miR-1307-3p promotes tumor growth and metastasis of hepatocellular carcinoma by repressing DAB2 interacting protein," *Biomedicine & Pharmacotherapy*, vol. 117, Article ID 109055, 2019.

[23] P. Yuan, J. Li, F. Zhou et al., "NPAS2 promotes cell survival of hepatocellular carcinoma by transactivating CDC25A," *Cell Death & Disease*, vol. 8, no. 3, p. e2704, 2017.

[24] Y. Yang, T. Yang, Z. Zhao et al., "Down-regulation of BMAL1 by MiR-494-3p promotes hepatocellular carcinoma growth and metastasis by increasing GPAM-mediated lipid biosynthesis," *International Journal of Biological Sciences*, vol. 18, no. 16, pp. 6129–6144, 2022.

[25] M. E. Ritchie, B. Phipson, D. Wu et al., "Limma powers differential expression analyses for RNA-sequencing and microarray studies," *Nucleic Acids Research*, vol. 43, no. 7, p. e47, 2015.

[26] S. Hänzelmann, R. Castelo, and J. Guinney, "GSVA: gene set variation analysis for microarray and RNA-seq data," *BMC Bioinformatics*, vol. 14, no. 1, p. 7, 2013.

[27] T. T. Liu, R. Li, C. Huo et al., "Identification of CDK2-related immune forecast model and ceRNA in lung adenocarcinoma, a pan-cancer analysis," *Frontiers in Cell and Developmental Biology*, vol. 9, Article ID 682002, 2021.

[28] P. Langfelder and S. Horvath, "WGCNA: an R package for weighted correlation network analysis," *BMC Bioinformatics*, vol. 9, no. 1, p. 559, 2008.

[29] A. Sharma, J. J. W. Seow, C. A. Dutertre et al., "Onco-fetal reprogramming of endothelial cells drives immunosuppressive macrophages in hepatocellular carcinoma," *Cell*, vol. 183, no. 2, pp. 377–394.e21, 2020.

[30] F. A. Wolf, P. Angerer, and F. J. Theis, "SCANPY: large-scale single-cell gene expression data analysis," *Genome Biology*, vol. 19, no. 1, p. 15, 2018.

[31] Z. Lv, F. Cui, Q. Zou, L. Zhang, and L. Xu, "Anticancer peptides prediction with deep representation learning features," *Briefings in Bioinformatics*, vol. 22, no. 5, 2021.

[32] Y. Liu, Y. Dong, X. Wu, X. Wang, and J. Niu, "Identification of immune microenvironment changes and the expression of immune-related genes in liver cirrhosis," *Frontiers in Immunology*, vol. 13, Article ID 918445, 2022.

[33] Z. Fang, X. Liu, and G. Peltz, "GSEApy: a comprehensive package for performing gene set enrichment analysis in Python," *Bioinformatics*, vol. 39, no. 1, 2023.

[34] H. Chi, X. Xie, Y. Yan et al., "Natural killer cell-related prognosis signature characterizes immune landscape and predicts prognosis of HNSCC," *Frontiers in Immunology*, vol. 13, Article ID 1018685, 2022.

[35] P. Martínez-Camblor and J. C. Pardo-Fernández, "Parametric estimates for the receiver operating characteristic curve generalization for non-monotone relationships," *Statistical Methods in Medical Research*, vol. 28, no. 7, pp. 2032–2048, 2019.

[36] X.-S. L. Shixiang Wang, J. Li, and Z. Qi, "Ezcox: an r/cran package for cox model batch processing and visualization," 2021, https://cran.r-project.org/web/packages/ezcox/index.html.

[37] X. Wu, W. Lu, C. Xu et al., "PTGIS may Be a predictive marker for ovarian cancer by regulating fatty acid metabolism," *Computational and Mathematical Methods in Medicine*, vol. 2023, Article ID 2397728, 13 pages, 2023.

[38] X. Pan, X. Jin, J. Wang, Q. Hu, and B. Dai, "Placenta inflammation is closely associated with gestational diabetes mellitus," *Am J Transl Res*, vol. 13, no. 5, pp. 4068–4079, 2021.

[39] D. D. Sjoberg, "Decision curve analysis for model evaluation," 2020, https://www.danieldsjoberg.com/dcurves/.

[40] P. Charoentong, F. Finotello, M. Angelova et al., "Pan-cancer immunogenomic analyses reveal genotype-immunophenotype relationships and predictors of response to checkpoint blockade," *Cell Reports*, vol. 18, no. 1, pp. 248–262, 2017.

[41] P. Jiang, S. Gu, D. Pan et al., "Signatures of T cell dysfunction and exclusion predict cancer immunotherapy response," *Nature Medicine*, vol. 24, no. 10, pp. 1550–1558, 2018.

[42] Y. Liu, C. Jiang, C. Xu, and L. Gu, "Systematic analysis of integrated bioinformatics to identify upregulated THBS2 expression in colorectal cancer cells inhibiting tumour immunity through the HIF1A/Lactic Acid/GPR132 pathway," *Cancer Cell International*, vol. 23, no. 1, p. 253, 2023.

[43] D. Maeser, R. F. Gruener, and R. S. Huang, "oncoPredict: an R package for predicting in vivo or cancer patient drug response and biomarkers from cell line screening data," *Briefings in Bioinformatics*, vol. 22, no. 6, 2021.

[44] Y. Han, L. Chen, L. Baiocchi et al., "Circadian rhythm and melatonin in liver carcinogenesis: updates on current findings," *Critical Reviews in Oncogenesis*, vol. 26, no. 3, pp. 69–85, 2021.

[45] G. Li, J. Zhang, D. Liu et al., "Identification of hub genes and potential ceRNA networks of diabetic nephropathy by weighted gene Co-expression network analysis," *Frontiers in Genetics*, vol. 12, Article ID 767654, 2021.

[46] C. Miro, A. Docimo, L. Barrea et al., "Time for obesity-related cancer: the role of the circadian rhythm in cancer pathogenesis and treatment," *Seminars in Cancer Biology*, vol. 91, pp. 99–109, 2023.

[47] P. Yuan, T. Yang, J. Mu et al., "Circadian clock gene NPAS2 promotes reprogramming of glucose metabolism in hepatocellular carcinoma cells," *Cancer Letters*, vol. 469, pp. 498–509, 2020.

[48] M. Crespo, M. Leiva, and G. Sabio, "Circadian clock and liver cancer," *Cancers*, vol. 13, no. 14, p. 3631, 2021.

[49] J. H. Oh, J. H. Lee, D. H. Han, S. Cho, and Y. J. Lee, "Circadian clock is involved in regulation of hepatobiliary transport mediated by multidrug resistance-associated protein 2," *Journal of Pharmaceutical Sciences*, vol. 106, no. 9, pp. 2491–2498, 2017.

[50] Y. Shen, M. Endale, W. Wang et al., "NF-κB modifies the mammalian circadian clock through interaction with the core clock protein BMAL1," *PLoS Genetics*, vol. 17, no. 11, 2021.

[51] T. Liu, Z. Wang, L. Ye et al., "Nucleus-exported CLOCK acetylates PRPS to promote de novo nucleotide synthesis and liver tumour growth," *Nature Cell Biology*, vol. 25, no. 2, pp. 273–284, 2023.

[52] D. Gu, S. Li, S. Ben et al., "Circadian clock pathway genes associated with colorectal cancer risk and prognosis," *Archives of Toxicology*, vol. 92, no. 8, pp. 2681–2689, 2018.
[53] P. B. Schwartz, M. Nukaya, M. E. Berres et al., "The circadian clock is disrupted in pancreatic cancer," *PLoS Genetics*, vol. 19, no. 6, p. e1010770, 2023.
[54] Z. Zhang, P. Zeng, W. Gao, Q. Zhou, T. Feng, and X. Tian, "Circadian clock: a regulator of the immunity in cancer," *Cell Communication and Signaling*, vol. 19, no. 1, p. 37, 2021.
[55] C. Scheiermann, Y. Kunisaki, and P. S. Frenette, "Circadian control of the immune system," *Nature Reviews Immunology*, vol. 13, no. 3, pp. 190–198, 2013.
[56] A. M. Curtis, M. M. Bellet, P. Sassone-Corsi, and L. A. O'Neill, "Circadian clock proteins and immunity," *Immunity*, vol. 40, no. 2, pp. 178–186, 2014.
[57] N. Labrecque and N. Cermakian, "Circadian clocks in the immune system," *Journal of Biological Rhythms*, vol. 30, no. 4, pp. 277–290, 2015.
[58] K. Man, A. Loudon, and A. Chawla, "Immunity around the clock," *Science*, vol. 354, no. 6315, pp. 999–1003, 2016.
[59] C. Scheiermann, J. Gibbs, L. Ince, and A. Loudon, "Clocking in to immunity," *Nature Reviews Immunology*, vol. 18, no. 7, pp. 423–437, 2018.
[60] R. Pick, W. He, C. S. Chen, and C. Scheiermann, "Time-of-Day-Dependent trafficking and function of leukocyte subsets," *Trends in Immunology*, vol. 40, no. 6, pp. 524–537, 2019.
[61] M. Palomino-Segura and A. Hidalgo, "Circadian immune circuits," *Journal of Experimental Medicine*, vol. 218, no. 2, Article ID e20200798, 2021.
[62] C. Wang, C. Barnoud, M. Cenerenti et al., "Dendritic cells direct circadian anti-tumour immune responses," *Nature*, vol. 614, no. 7946, pp. 136–143, 2023.
[63] S. Sahar and P. Sassone-Corsi, "Metabolism and cancer: the circadian clock connection," *Nature Reviews Cancer*, vol. 9, no. 12, pp. 886–896, 2009.